On the development of effective heave pressure in deep excavations

Downloaded from: https://research.chalmers.se, 2026-10-07 04:06 UTC

Citation for the original published paper (version of record):
Tornborg, J., Karlsson, M., Dijkstra, J. et al (2025). On the development of effective heave pressure in deep excavations. Geotechnique, 75(13): 181-194. http://dx.doi.org/10.1680/jgeot.24.01066

N.B. When citing this work, cite the original published paper.

research.chalmers.se offers the possibility of retrieving research publications produced at Chalmers University of Technology. It covers all kind of research output: articles, dissertations, conference papers, reports etc. since 2004. research.chalmers.se is administrated and maintained by Chalmers Library

(article starts on next page)

Tornborg, J. *et al.* (2025). *Géotechnique* **75**, No. 13, 181–194 [https://doi.org/10.1680/jgeot.24.01066]

On the development of effective heave pressure in deep excavations

JOHANNES TORNBORG*, MATS KARLSSON†, JELKE DIJKSTRA‡ and MINNA KARSTUNEN§

The processes and factors that underpin the development of effective heave pressure (EHP) at the base of deep excavations in soft soils have been numerically quantified for two idealised soil–structure systems, namely, a building unit cell and a tunnel geometry, using the finite-element method. Charts were developed exploiting dimensional analysis to estimate the impact of normalised time between the end of excavation and the completion of the restraining structure at the base, on the emerging magnitude of EHP for several scenarios where the excavation geometry, ground profile, relative stiffness and retaining wall length were varied. The results of the analyses were in good agreement with available data from physical model tests and the monitoring data of a deep excavation in Gothenburg, Sweden. Complementary analyses of site-specific background settlements and water table levels demonstrate that the charts developed are conservative. The results of this study can, within the limitations of the scenarios studied, readily be used for estimations of EHP in the preliminary design stage, and as a complement to detailed, project-specific analyses.

KEYWORDS: clays; earth pressure; excavation; numerical modelling; soil/structure interaction

INTRODUCTION

Urbanisation and sustainable development drives the increasing need to utilise underground space (Broere, 2016; UN, 2019), calling for accurate predictions of the magnitude of the actions on the structures. Such actions include the temporal evolution of earth pressures on temporary and permanent retaining structures, underground structures and below the base of excavations. While the development of lateral earth pressures on underground and retaining structures in soft soils has been widely studied (e.g. Peck, 1943; Flaate, 1966; Peck, 1969; Finno *et al*., 2002; Karlsrud & Andresen, 2005; Ng *et al*., 2012; Whittle *et al*., 2015; Rouainia *et al*., 2017; Schweiger & Tschuchnigg, 2021), this is not the case for the development of earth pressures below structures at the base of deep excavations in soft clays.

At the base of deep excavations in soils with a low permeability (hydraulic conductivity) a delayed unloading response is observed (e.g. Symons & Tedd, 1989; Nash *et al*., 1996; Chan *et al*., 2018). The negative excess pore pressures (suction) that are initially generated during the excavation, slowly dissipate with time, leading to the heave of the excavation bottom. Considerable loads on the structural elements at the base can be mobilised in situations where this dissipation process has not yet finished at the time of construction of structural elements that restrain the heave. An example is a base slab fixed by tension piles, anchors or heavily loaded columns or walls (Price *et al.*, 1986; Chan *et al*., 2022a).

The quantification of excavation-induced heave pressures (e.g. Burland & Kalra, 1986) that are restrained by structural elements remains challenging. Simpson (2018) showed that the industry practice outlined in Ingram (2012) for the calculation of earth pressure due to restrained heave is inadequate. Soil–structure interaction effects need to be explicitly incorporated in the design method, to properly assess the effective heave pressure (EHP) acting on the structure due to restrained heave. Hence, the relative stiffness between the structural element and the soil is an important factor in the system response (Chan *et al*., 2022a, 2022b).

The effect of the time between the end of excavation, and the installation of the structure that restrains the heave, affecting the magnitude of EHP, has not been explicitly studied in prior work. Consequently, in most studies only a single case for normalised time T is investigated. System-level effects, such as the magnitude of excess pore water pressure induced by excavation (Bertoldo & Callisto, 2019) and the geometry of the excavation in relation to the depth of the clay layer (Christian & David Carrier III, 1978), on the temporal development of EHP remain poorly understood. Furthermore, EHP might further evolve during the service life of an underground structure in soft soils with ongoing creep-driven deformations. Clearly, the estimation of EHP depends on many factors including the geometry, soil properties, construction time and the type of restraint (structural elements at the base and sides of the excavation).

This study overcomes the uncertainties in the assessment of the magnitude of EHP and its evolution with time, by developing a set of charts to evaluate EHP. The novelty lies in the extensive automated numerical parametric study, using the finite-element method, designed and evaluated with the aid of dimensionless groups. The results are applicable for a wide range of settings for lightly overconsolidated clays of varying thickness, as well as various excavation geometries, construction time, soil stiffness and permeability. Therefore, the results can readily be used for estimations of EHP in preliminary design stages and as a complement to detailed project-specific analyses.

Manuscript received 8 April 2024; revised manuscript accepted 24 July 2024.
Discussion on this paper closes 1 May 2026; for further details see p. ii.
Published with permission by Emerald Publishing Limited under the CC-BY 4.0 license. (http://creativecommons.org/licenses/by/4.0/)
* Department of Architecture and Civil Engineering, Chalmers University of Technology and Skanska Sweden AB, Gothenburg, Sweden (Orcid:0000-0002-9232-2474).
† Department of Architecture and Civil Engineering, Chalmers University of Technology, Gothenburg, Sweden (Orcid:0000-0002-7417-5765).
‡ Department of Architecture and Civil Engineering, Chalmers University of Technology, Gothenburg, Sweden (Orcid:0000-0003-3792-0727).
§ Department of Architecture and Civil Engineering, Chalmers University of Technology, Gothenburg, Sweden (Orcid:0000-0002-5401-5721).

Downloaded from http://www.emerald.com/jgeot/article-pdf/75/13/181/10972300/jgeot.24.01066en.pdf by Chalmers University of Technology user on 10 June 2026

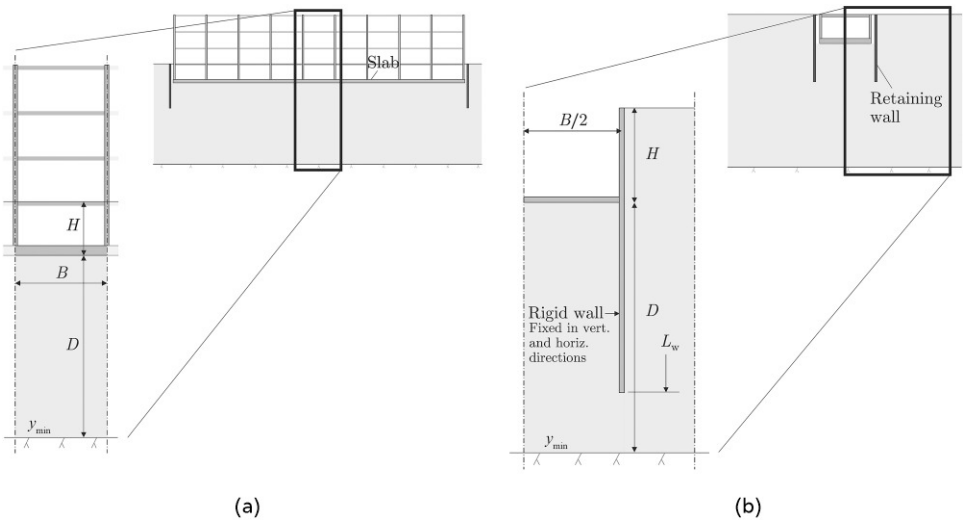

Fig. 1. Idealised soil–structure systems considered in the parametric study: (a) building unit cell (BUC); (b) tunnel

NUMERICAL QUANTIFICATION OF EFFECTIVE HEAVE PRESSURE

Variables considered and dimensionless groups

The development of EHP at the base of deep excavations is an interaction between the generation of (negative) excess pore pressures during excavation, the subsequent dissipation of pore pressures that result in basal heave and the impact of the structural elements (and their properties) at the base and sides of the excavation. Hence, EHP at the base of excavations in soft soils are impacted by the following factors: (*a*) the soil–structure interaction that underpins the relative displacement and stiffness between the structure and adjacent soil; (*b*) the time of placement of the structural restraint after completion of excavation (pore pressure dissipation as a function of normalised time); and (*c*) the geometry of the excavation in relation to the depth of the clay layer (affecting the ratio of immediate to delayed heave and the subsequent rate of pore pressure dissipation as a function of drainage conditions). In the absence of a comprehensive experimental data set, numerical analyses will be used to conduct a parametric study to investigate the impact of the above factors on the magnitude and temporal evolution of EHP. Furthermore, the complexity of the parametric study is increased sequentially, where the most advanced scenarios capture more advanced soil response and more complex geometries, that is: (*a*) model geometry, moving from a one-dimensional (1D) *building unit cell* to a case considering a two-dimensional (2D) excavation for a *tunnel* (as defined later in the section 'Numerical model'); (*b*) soil model, moving from the linear elastic–perfectly plastic Mohr–Coulomb (MC) model, to the SClay1S (Karstunen *et al*., 2005) and Creep-SClay1S (Sivasithamparam *et al*., 2015; Gras *et al*., 2018) models, which are more applicable for soft natural clays. In the scenarios simulating a tunnel geometry, the retaining wall is considered as rigid, and thus only the wall length L_w is varied to control the basal stability of the excavation.

The main driver for EHP is the incomplete dissipation of excess pore pressures that were generated during excavation, at the time that the structural restraint is activated. The magnitude of the generated excess pore pressure is governed by the excavation depth H and the unit weight γ of the excavated soil. The dissipation is controlled by the bulk stiffness and the permeability of the soil, that is, the (vertical) coefficient of consolidation c_v, and the drainage length D. Hence, the magnitude of EHP is strongly linked to the time $t_{exc.-slab}$ between the end of excavation and the placement of the structural element at the base of the excavation. The time for excavation is idealised in this study, being completed in ≤7 days. The motivation for this assumption was to simulate a short excavation process, resulting in a conservative value for the computed EHP, compared to practical times for excavation processes within deep excavations.

The deflection of the structural element, considering here a bottom slab, at the base of the excavation (due to EHP and water pressure) is controlled by the span B and the rigidity EI_{slab} of the slab relative to the stiffness of the soil E_{soil}. From the above reasoning and idealisations, EHP is considered to be dependent on the following variables:

$$\mathrm{EHP} = f(\gamma, H, E_{slab}, I_{slab}, E_{soil}, B, t_{exc.-slab}, c_v, D) \quad (1)$$

which can be further arranged into the following dimensionless groups:

$$\frac{\mathrm{EHP}}{\gamma H} = f\left(\frac{EI_{slab}}{E_{soil}B^3}, \frac{c_v t}{D^2}\right) \quad (2)$$

It should, however, be noted that the total (effective) rigidity of the structural restraint may increase progressively during construction, and depends on the type of sub- and superstructure, including the location of walls within the slab (Brown & Yu, 1986; O'Brien *et al*., 2012).

EHP is considered as an earth pressure in addition to any permanent water pressure. Therefore, EHP should be related to a portion of γH-u_0, that is σ'_{v0} at the excavation level. For a rigid structure, the upper limit of the uplift pressure would be the vertical effective stress at that level prior to excavation. Equation (2) then becomes

Table 1. Mohr–Coulomb model parameter values

Parameter	Fill	Clay
γ/γ': kN/m^3	16/6	16/6
E: MPa	20	Varying
ν'	0·3	0·2
c': kPa	1	1
ϕ': degrees	35	30
ψ': degrees	0	0
K_0	$1 - \sin\phi'$	0·6

Downloaded from http://www.emerald.com/jgeot/article-pdf/75/13/181/10972300/jgeot.24.01066en.pdf by Chalmers University of Technology user on 10 June 2026

Table 2. SClay1S and Creep-SClay1S model parameter values

Parameter	Description	SClay 1S	Creep-SClay 1S†
γ/γ' : kN/m^3	Unit weight	16/6	16/6
λ_i	Intrinsic compression index	0·19	0·07 (λ_i^*)
κ	Swelling index	0·014	0·005 (κ^*)
ν'	Poisson's ratio	0·20	0·20
M_c	Slope of CSL in triaxial compression	1·45	1·45
M_e	Slope of CSL in triaxial extension	1·1	1·1
ω	Rate of rotational hardening	200	200
ω_d	Relative rate of rotational hardening	1	1
a	Rate of destructuration	8	8
b	Relative rate of destructuration	0·5	0·5
α_0	Initial anisotropy	0·57	0·57
χ_0	Initial amount of bonding	15	15
μ_i^*	Modified intrinsic creep index	—	1/550‡
τ : days	Reference time	—	1
K_0^{nc}§	Earth pressure coefficient at primary loading	0·42	0·42

†Operates on *modified* compression, swelling and creep indices.
‡1/800 below 20 m depth in scenario 6 (see section 'Impact of background settlements').
§From $K_0^{nc} = 1 - \sin\phi'$ with $\phi' = \phi'_{CSLc}$.

$$\frac{EHP}{\sigma'_{v0}} = f\left(\frac{EI_{slab}}{E_{soil}B^3}, \frac{c_v t}{D^2}\right) \quad (3)$$

The left-hand side of equation (3) is the EHP ratio, the first term of the right-hand side is a relative stiffness ratio, R, and the second term is the normalised time, or time factor T_v. Some aspects of the excavation and loading history in the soil will further impact the EHP. Hence, in addition to the variables in equation (3), the parametric study will generalise the effect of: (*a*) varying the increase of soil stiffness with depth; (*b*) excavation stability by varying the retaining wall length; (*c*) varying the self-weight of the structural element; (*d*) background settlements; and (*e*) the location of the groundwater table.

Numerical model

Two idealised soil–structure systems are studied in the finite-element analysis, see Fig. 1. In the first case, a plane strain *building unit cell* (BUC) is considered, where the impact of the retaining wall and the extent of the excavation are not considered. In the second idealisation of a *tunnel geometry*, the retaining wall is also incorporated. The slab is modelled as a plate element with a linear elastic constitutive model considering the intact stiffness of the concrete (ignoring cracks). Once activated, the element is fixed (clamped) at the model boundaries in the BUC. For the *tunnel geometry*, the simulations are restricted to a rigid slab. This aids in isolating the impact of more realistic soil conditions (impact of soil model, background settlements and location of the groundwater table). In reality, the EHP and any water pressure are likely to mobilise some upward displacement of the structure. As a result, these idealisations contribute to conservative outputs of computed EHP. To normalise the structural response from EHP, the bending moment M in the BUC is normalised to

$$\frac{M}{\gamma HB^2} \quad (4)$$

The heave δ_v of the structural element or the base of the excavation in the BUC is also normalised to

$$\frac{\delta_v E_{soil}}{\gamma HD} \quad (5)$$

where δ_v is the vertical displacement; E_{soil} in the unit cell geometry is the constrained oedometer modulus; E_{oed}, derived from $E_{oed} = E_{soil}(1-\nu')/((1+\nu')(1-2\nu'))$ with $\nu' = 0{\cdot}2$. For the *tunnel geometry* the (effective) Young's modulus E_{soil} is used. The retaining wall and the vertical model boundaries are modelled as impermeable. The lower model boundary, as well as the interface at the excavation base and structural element, are considered as permeable. The motivation for the latter idealisation is that in practice a coarse-grained layer is typically used to level the excavation base before casting of a concrete slab.

Constitutive models

Analyses are initially carried out using the linear elastic–perfectly plastic MC model. Table 1 provides the parameter values used for the clay deposit and the top layer of fill material (thickness of 1 m unless stated otherwise). Subsequently, the SClay1S and Creep-SClay1S models are used, to represent the emerging response of a lightly overconsolidated natural clay. Specifically, the latter model allows the effect of background creep settlements on the evolution of EHP to be quantified. Table 2 summarises the values for the model parameters used in this study for a representative Swedish soft sensitive clay (Tornborg *et al.*, 2021).

The coefficient of earth pressure at rest, K_0, is set to 0·6 and for the SClay1S and Creep-SClay1S models, the

Table 3. Calculation phases in the finite-element analyses

Phase	Description	Time: days
1	Activation of SPWs	1
2	Excavation	1–7
3	Stall-time (construction)	Varied ($t_{exc.-slab}$)
4	Apply line load simulating wet concrete*	1
5	Deactivate line load*, activate slab	0–1
6	*Stall-time (construction)*	*Varied (90 and 3650)*
7	*End of dewatering, start return of steady state pore pressures*	*730*
8	Consolidation	Varies†

*In scenarios 2 and 6.
†Until $u_{excess,max} < 1$ kPa.
Note: Italic font indicates cases involving a groundwater table located at 1 m depth b.g.l.

Downloaded from http://www.emerald.com/jgeot/article-pdf/75/13/181/10972300/jgeot.24.01066en.pdf by Chalmers University of Technology user on 10 June 2026

Table 4. Summary of studied scenarios

Scenario	Geometry	Soil model	Parameter variation								
			H: m	G.w.t. location	$t_{exc.-slab}$: days	y_{min}: m	E_{soil}: MPa	k : m/s	B‡ : m	w: kPa	L_w: m
1 Fig. 3	BUC†	Mohr–Coulomb	5	Exc. base	1, 10, 30, 90, 365, 1825, 3650	35	22	10^{-9}	2·5(△), 5(+), 8(○), 11(□), 17 (▽), 25 (×)	0‡	–
2 Figs 4–7	BUC	Mohr–Coulomb	5, 10, 15	Exc. base	1, 10, 90, 365, 912, 1825, 3650	35	22	0·4–1·0 × 10^{-9}	2·5(△), 5(+), 8(○), 11(□), 17 (▽), 25(×), 50(◇), 200(☆)	25‖	–
3 Fig. 8	Tunnel	Mohr–Coulomb	5, 10	Exc. base	1	20, 25, 50, 75, 100	22 + 0·5/m 22 + 2·0/m¶	10^{-6}, 10^{-7}, 10^{-8}, 10^{-9}, 10^{-10}, 10^{-11}	10(□), 25(◁), 50(◇), 100(▷)	0	6, 10, 15, 30
4 Fig. 9	Tunnel	SClay1S†† and Creep-SClay 1S	5, 10‡‡	Exc. base	5, 30, 90, 365	25, 50, 75, 100	κ = 0·014 κ^* = 0·005 κ^* = 0·015§§	10^{-9}	10(□), 25(◁), 50(◇)	0	15, 25**
5 Figs 10, 11	Tunnel	Creep-SClay1S	5	Exc. base	90	90	κ^* = 0·005	10^{-9}	25(◁), 35(+), 50(◇), 75(▽), 100(▷)	0	15
6 Figs 12, 13	Tunnel	SClay1S and Creep-SClay1S	5	1 m b.g.l.	5, 30, 70, 90, 365	50(○), 75(▷), 90(▽)	κ = 0·014 κ^* = 0·005	10^{-9}	25	0, 25‖‖	15

†BUC = building unit cell.
‡Symbols within brackets indicate marker symbols in figures.
§EI_{slab} = 313 MNm^2.
‖EI_{slab} = 2500 MNm^2.
¶Indicated by filled symbols in Fig. 8.
††Indicated by filled symbols in Fig. 9.
‡‡Indicated by half-filled symbols in Fig. 9.
§§Creep-SClay 1S simulations with different κ^* (κ^* = 0·015 simulations indicated by thin marker edge lines in Fig. 9).
‖‖In the Creep-SClay1S simulation.
Note: Text colour indicates colour used for markers in figures.

Downloaded from http://www.emerald.com/jgeot/article-pdf/75/13/181/10972300/jgeot.24.01066en.pdf by Chalmers University of Technology user on 10 June 2026

overconsolidation ratio, $OCR = 1{\cdot}3$. The permeability of the soil is varied in the parametric study; however, it is idealised as uniform and isotropic. For the simulations using the MC model, the interfaces between the clay and the structural elements are modelled with an interface factor, $R_{inter} = 0{\cdot}5$. For the SClay1S and Creep-SClay1S models, the interfaces are modelled assuming full friction with $\phi' = 35°$ and $c' = 1$ kPa. The effect of the slab interface material on the magnitude of the EHP was investigated by running simulations with the Creep-SClay1S model (*tunnel geometry* with $H = 10$ m) adopting the MC material interface settings. The computed EHP increased by a factor of 1·002–1·005 (maximum difference 0·5 kPa) when using the MC interface, suggesting a negligible impact on the results.

Finite-element analyses

The calculation phases are outlined in Table 3. Simulations involve groundwater tables located at (*a*) the excavation base and (*b*) at 1 m depth below ground level. For situation (*a*), the analyses are performed using a decoupled consolidation analysis ('Consolidation' calculation type in Plaxis 2D version 21·01·00·479). For situation (*b*), fully coupled analyses are performed to accommodate a temporary groundwater lowering and change of steady state pore pressures during the construction stage. In all cases the soil is considered as fully saturated with no suction cut-off. Table 4 presents an overview of the simulated scenarios in the parametric study and the range for the parameter variation. Scenarios 1 and 2 concern the BUC considering a weightless slab and a slab with a self-weight of 25 kPa, respectively. Scenarios 3–6 concern the tunnel geometry and quantify, for example, the effect of soil model, background settlements and a high groundwater table on the computed EHP. The MC model is used in scenarios 1–3 and the SClay1S and Creep-SClay1S in scenarios 4–6. A representative finite-element mesh used in this study is illustrated in Fig. 2.

RESULTS AND DISCUSSION

Building unit cell – MC model

Impact of normalised time and relative stiffness. First, a simple scenario of the BUC involving a weightless slab, and a groundwater table located at the excavation base, is analysed with the MC model (i.e. scenario 1 in Table 4). The following findings for the soil–structure response and development of EHP can be observed.

(*a*) The hogging displacement of the slab (Fig. 3(a)) increases with decreasing normalised time T and relative stiffness ratio R. This is reflected in the distribution of the action, EHP, along the slab (Fig. 3(b)). For low R, EHP will be non-uniform with the fixed edges of the slab attracting load from the central part. For $R < 0{\cdot}1$ this results in EHP at the location of the wall being higher than the in situ vertical effective stress. For illustration, centrifuge test results (for a flexible slab (Chan *et al.*, 2022b)) are normalised and included in Fig. 3(b).

(*b*) Figure 3(c) shows that the dissipation of EHP with T is a process of reversed consolidation settlement. In this figure, $1 - U$ illustrates an analytical solution (Muir Wood, 2009) to Terzaghi's theory of 1D consolidation.

(*c*) Figures 3(c) and 3(d) quantify how EHP at the centre of the slab reduces with increasing T and/or decreasing R.

(*d*) In addition to EHP in any part of the slab, the structurally more relevant bending moment is also computed. Fig. 3(e) quantifies the wall and central moment as a function of R and T. The decrease in bending moment comes at the expense of increasing differential slab displacements (indicated by the shaded results, plotted against the vertical axis on the right).

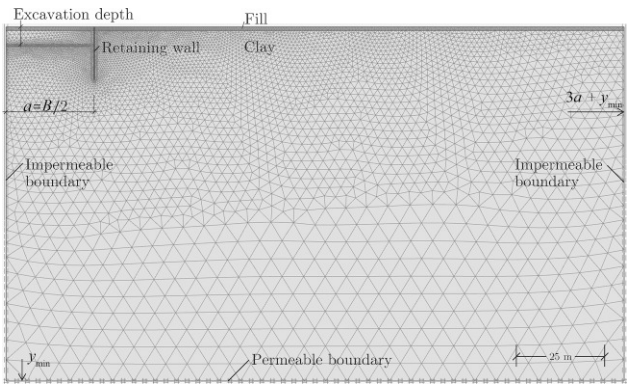

Fig. 2. Example of a finite-element mesh (from scenario 4) consisting of six-noded triangular elements (10 731 elements in this example)

Impact of excavation depth and self-weight of the slab. Figure 4 extends on the previous results by introducing the effect of a self-weight, w, of the slab.

A slab with $w = 25$ kPa is considered for $H = 5$, 10 and 15 m, to generalise this effect in relation to H. Fig. 5 illustrates for $H = 5$ m the normalised displacement of the excavation bottom and slab plotted against the normalised time. Combined, Figs 4 and 5 provide the following insights.

- For low R ($\leq 10^{-3}$), the minimum vertical earth pressure corresponds to the self-weight.
- For high R ($>10^{-1}$) the slab is able to bridge across the supports and does not impose any pressure.
- If the heave has dissipated before the slab is cast, the self-weight may result in settlement (sagging) of the slab in systems with low R. To estimate the displacement pattern (sagging, or hogging due to EHP) one can study when the computed results intersect the illustration of $1 - U$, that is at $T = 0{\cdot}4$ and 0·9 for $H = 5$ and 15 m in Figs 4(a)–4(b).
- For low R, the long-term normalised displacement of the excavation bottom and slab approaches an asymptotic value, annotated in Fig. 5 for $H = 5$ m.

Figure 6(a) exemplifies the displacement of the slab when $H = 15$ m and Fig. 6(b) the distribution of the bending moment M for $H = 5$, 10 and 15 m. The intention here is not to illustrate distinguishable results of individual simulations, but rather to demonstrate that the results fall in place when normalised, as in Fig. 6(c), presenting the normalised bending moment ratio M/M_{wall} along the slab for $H = 5$, 10 and 15 m. For $R \geq 7 \times 10^{-3}$, the system resembles the behaviour of a rigid beam with uniform load, $R = 9 \times 10^{-4}$ behaves intermediate and $R = 10^{-5}$ as 'flexible' (centre of slab being flat). The absolute bending moments along the slab can be obtained by multiplying the normalised bending moment ratio with M_{wall} from Fig. 7. In Fig. 7, $H = 5$ m is separately plotted from $H = 10$ and 15 m, given for $H = 5$ m the slab self-weight results in marked settlement for $T > 3 \times 10^{-1}$ and larger bending moments (in sagging) compared to $H = 10$ and 15 m.

Downloaded from http://www.emerald.com/jgeot/article-pdf/75/13/181/10972300/jgeot.24.01066en.pdf by Chalmers University of Technology user on 10 June 2026

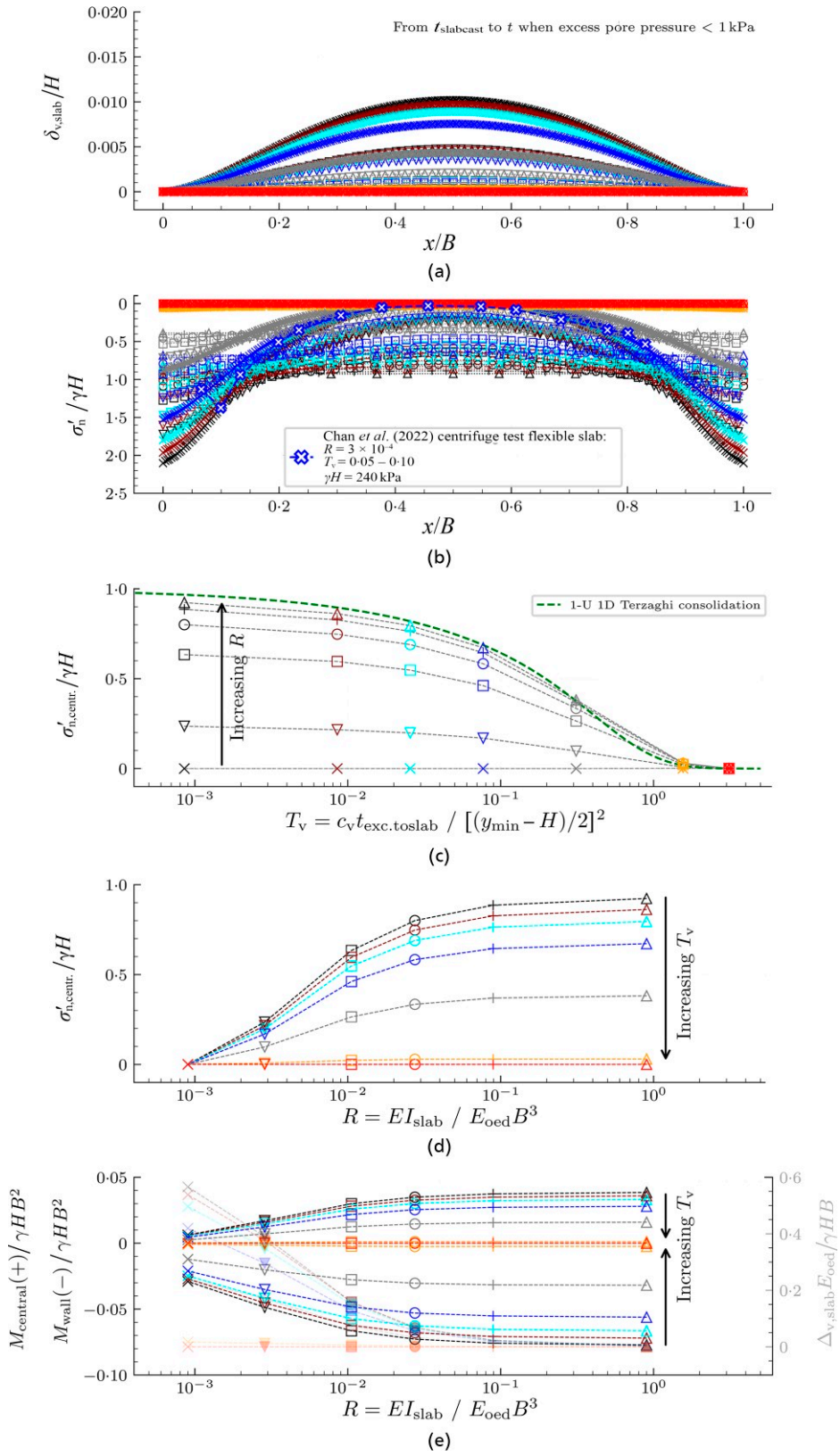

Fig. 3. Scenario 1: impact of T and R on: (a) slab displacement; (b) EHP along the slab; (c), (d) central EHP; and (e) central and wall bending moments, as well as differential slab displacement

Tunnel geometry

Three considerations arise when moving from the BUC to the *tunnel geometry*: (*a*) the proportion of the immediate to total heave is affected by the geometry of the excavation and the clay layer – in a similar way to the settlement influence factors for shallow foundations; (*b*) the consolidation of excavation-induced excess pore pressures is no longer 1D; (*c*) the reduced basal stability of the excavation contributes to heave and thereby affects the excess pore pressures.

Impact of system geometry: influence factor and 2D consolidation. Figure 8 shows the predicted EHP at the centre of a rigid restraint. The results have been normalised

Downloaded from http://www.emerald.com/jgeot/article-pdf/75/13/181/10972300/jgeot.24.01066en.pdf by Chalmers University of Technology user on 10 June 2026

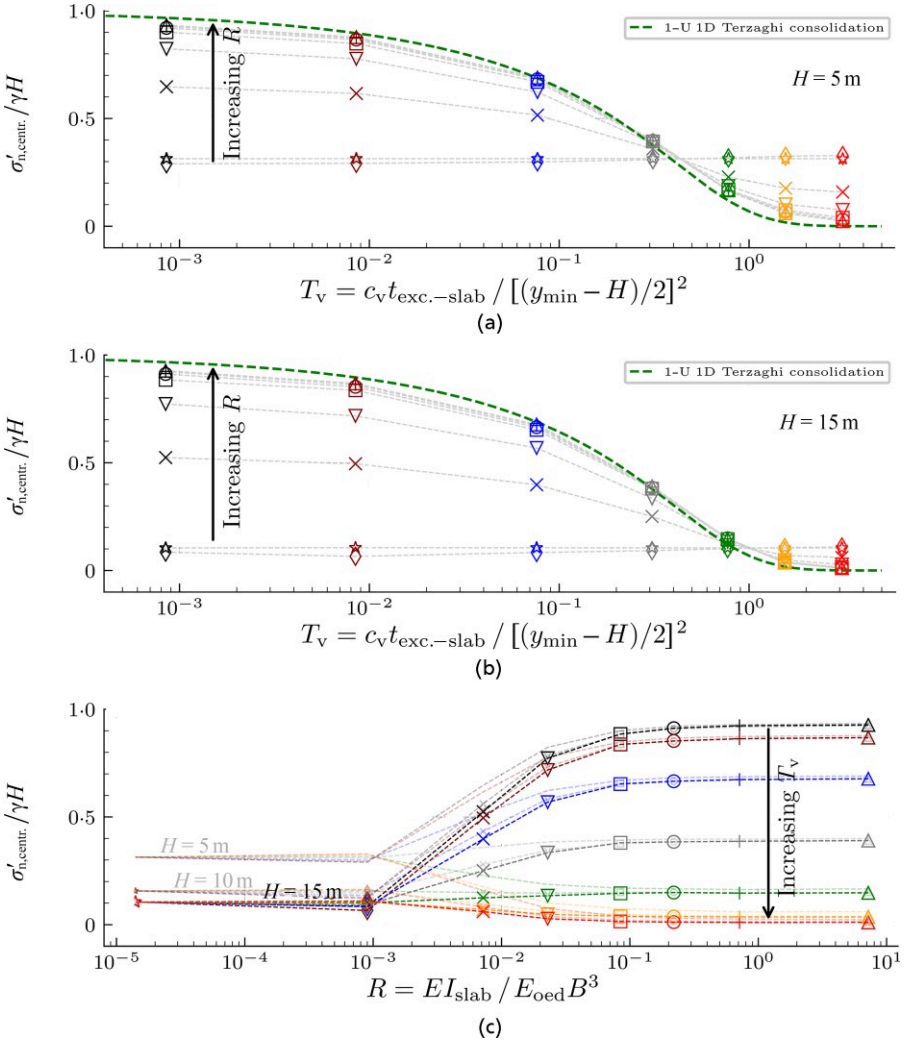

Fig. 4. Scenario 2: impact of slab self-weight, *w*, on EHP in relation to excavation depth: (a), (b) plotted against *T*; (c) plotted against *R*

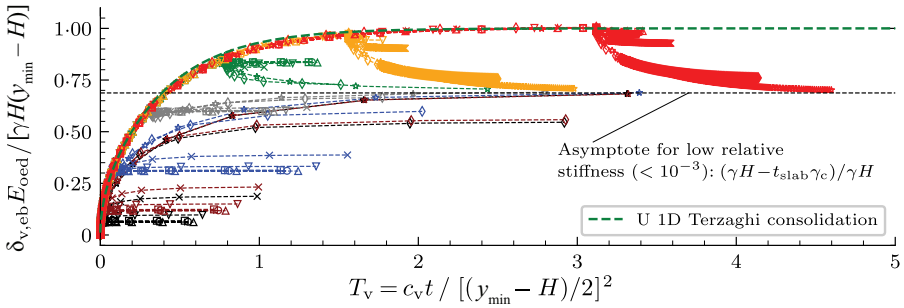

Fig. 5. Scenario 2: impact of slab self-weight, *w*, on normalised heave of the excavation bottom and slab (central part), plotted against *T* for *H* = 5 m

to the stiffness in the midpoint of the clay layer (between the excavation base and lower model boundary). As opposed to the BUC, the EHP ratio does not converge to 1 for small values of T, considering that, in a 2D problem, a portion of the heave occurs immediately due to shear strains in the soil during excavation. The magnitude of instant heave vanishes as the problem converges to conditions that are similar to the case of the BUC. Results from the simulations with small T are replotted in Fig. 8(b) to highlight this geometry effect. Clearly, the ratio of excavation width to the depth of the clay layer influences EHP, and an influence factor μ_i is proposed for normalisation. In Fig. 8(c), the results of Fig. 8(a) are replotted using a different expression for the normalised time that includes a horizontal component, that is:

$$T_{2D} = \left\{ c_v t_{exc.-slab} / \left[(y_{min} - H)/2 \right]^2 + (2B/y_{min}) c_h t_{exc.-slab} / (B/2)^2 \right\} / 2 [-] \quad (6)$$

The improved normalisation of the results for 2D effects using T_{2D} according to equation (6) (setting $c_h = c_v$), and the influence factor μ_i, are shown in Fig. 8(d).

Downloaded from http://www.emerald.com/jgeot/article-pdf/75/13/181/10972300/jgeot.24.01066en.pdf by Chalmers University of Technology user on 10 June 2026

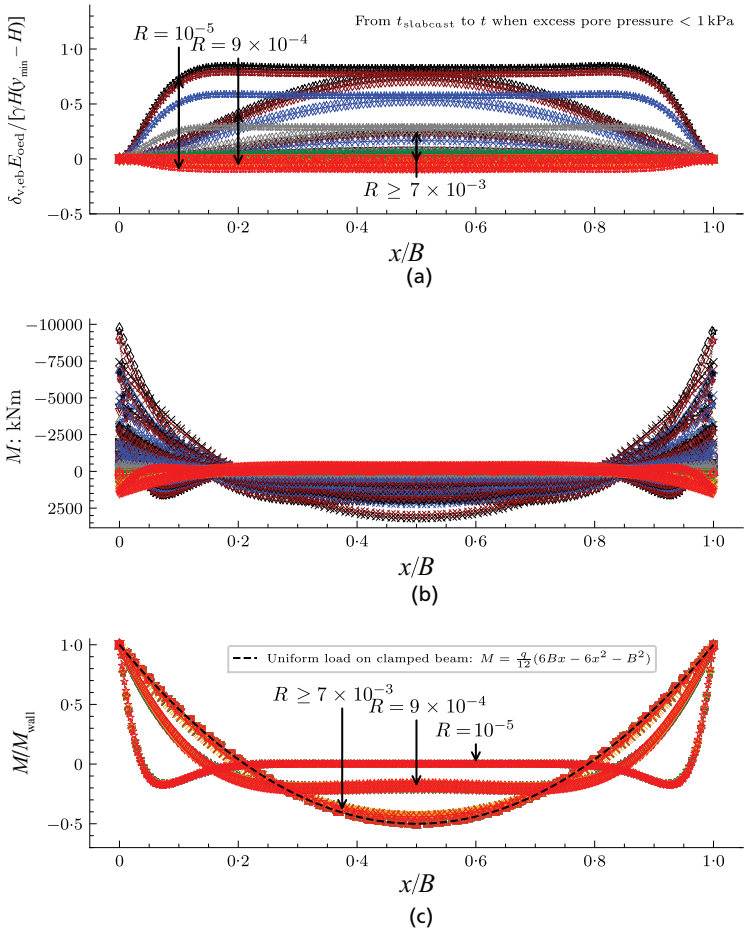

Fig. 6. Scenario 2: displacement and actions along the slab: (a) normalised vertical displacement for H = 15 m; (b), (c) bending moment and bending moment ratio, respectively, for H = 5, 10 and 15 m

Impact of retaining wall length. Two outliers are evident in Fig. 8(d) with the normalised EHP ratios of approximately 1·3. These outliers are simulations for H = 10 m, B = 10 m with L_w = 30 m. In this case the system represents a narrow deep excavation ($B < L_w$) and approximates the 1D BUC case. The opposite case, that is short walls leading to reduced basal stability, are exemplified in Fig. 8(d) for H = 5 m with EHP ratios reducing by a maximum of 20%. For large T, smaller negative excess pore pressure remain to be dissipated. Hence, the EHP ratio at the centre of the slab is not significantly affected. The loss of stability may, however, create an upward earth pressure close to the retaining wall. This effect is, however, not studied in the current paper, but can be considered as a reversed bearing capacity problem.

Impact of soil model. The SClay1S and Creep-SClay1S models enable the behaviour of natural clays to be captured (Karstunen *et al.*, 2005; Sivasithamparam *et al.*, 2015; Gras *et al.*, 2017) more accurately than the MC model. A major difference to the MC model is that the stiffness is anisotropic and stress dependent; furthermore, Creep-SClay1S accounts for rate-dependency. Fig. 9 presents the results of the tunnel geometry (scenario 3) re-analysed with SClay1S and Creep-SClay1S. Note, the groundwater table is (still) located at the excavation base. The results have been normalised using the initial stiffness in the midpoint of the clay layer. For the Creep-SClay1S results, the plotted EHP is the computed maximum value during the service life (as the earth pressures beneath the slab are evolving due to consolidation and rate-dependency). The results of the SClay1S model and maximum values computed by the Creep-SClay1S model are similar, also in comparison to the results using the MC model (scenario 3). The Creep-SClay1S model, however, allows the effects of rate-dependency (such as creep and relaxation) to be incorporated. The long-term (120 years) values computed by the Creep-SClay1S model are included in Fig. 9 as lightly shaded grey markers. As seen in Fig. 9(b), the long-term reduction of EHP clearly depends on the width of the excavation in relation to the depth of the clay layer. The effect of rate-dependency on long-term EHP is discussed further in section 'Impact of background settlements'.

COMPARISON TO PHYSICAL MODEL TESTS

The validity of the previously presented charts is assessed against well-documented physical model tests (Chan *et al.*, 2022a). Furthermore, this section serves as a worked example for their use. The model tests were performed at 100***g*** in a geotechnical centrifuge. The tests modelled a 15 m deep excavation in a 16 m deep overconsolidated (OCR of 2–3) clay layer overlain by 15 m of sand. The groundwater table was located at the excavation base. Table 6 in the Appendix specifies the prototype conditions, the evaluated parameters and the values of dimensionless groups for the benchmarking of the finite-element parametric study. Table 5 presents the EHP ratio and the normalised bending moment derived using the previously presented charts, compared to the physical model tests. The comparison is complicated by a load imposed on the basement walls 15 weeks after excavation in the model test. The 22 MN load equals 49 kPa if the load was to be distributed equally in the basement box. This caused the slab to

Downloaded from http://www.emerald.com/jgeot/article-pdf/75/13/181/10972300/jgeot.24.01066en.pdf by Chalmers University of Technology user on 10 June 2026

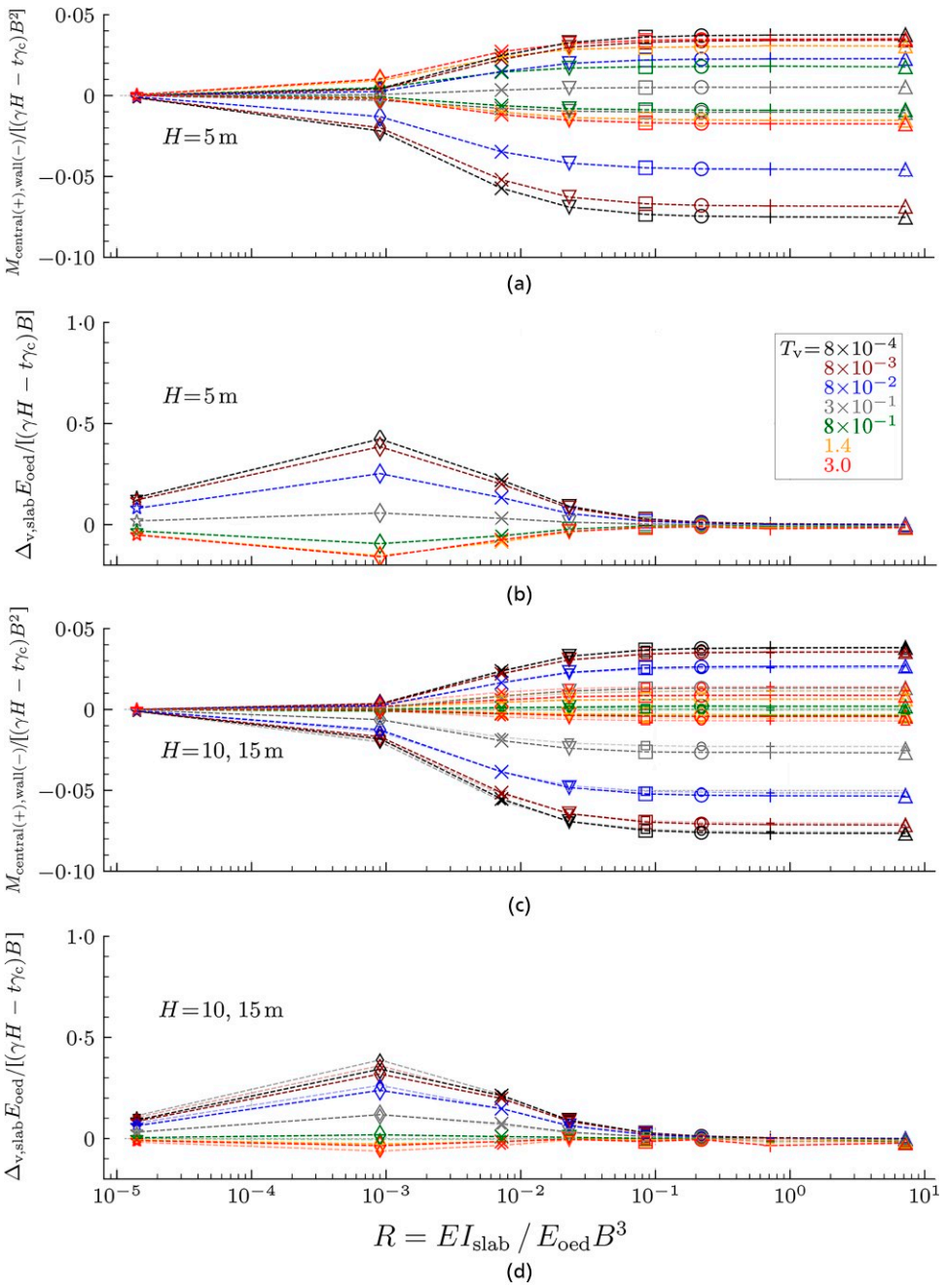

Fig. 7. Scenario 2: bending moment and differential displacement of slab as a function of T and R: (a), (b) H = 5 m; (c), (d) H = 10 (small markers) and 15 m. See subplot in (b) for the values of T

settle (Fig. 8(b) in Chan *et al.* (2022a)). Hence, after imposing the load it is unlikely that the slab contact pressure and bending moment are purely due to EHP. The reported central EHP ratio before load application was 0·45, and the normalised central moment was 0·022. The long-term results were included in Chan *et al.* (2022b), reporting an EHP ratio of 0·57, and the normalised central moment of 0·039. The agreement between the results of this parametric study and the model test is good until load application, but deviates in the long term. This suggests that the long-term observations in the physical model test are not purely due to EHP.

SITE-SPECIFIC CONDITIONS

Impact of background settlements

The charts in Figs 3–9 have been developed in a manner to avoid site-specific conditions. In deposits of soft clay with (historic) fills, however, background creep settlements are common. A representative (simplified) case in central Gothenburg, Sweden, is used to show the implication of background creep on the development of EHP. Here the ongoing settlements stem from historic land reclamation works, approximately 200 years ago, on the deep deposit of soft sensitive clay (for details see Tornborg *et al.* (2024)). The construction of 2 m of fill on top of the clay layer is simulated (a 1 year phase) followed by 200 years of consolidation, to initialise the settlement rates prior to excavation. Then, calculation phases as previously described (Table 3) are applied.

Figure 10 presents the computed settlement rate and the excess pore pressures in the clay deposit prior to construction for two scenarios (data on the previously presented scenario 4 are also included). In scenario 5 the groundwater table is located at the excavation base, whereas for scenario

Downloaded from http://www.emerald.com/jgeot/article-pdf/75/13/181/10972300/jgeot.24.01066en.pdf by Chalmers University of Technology user on 10 June 2026

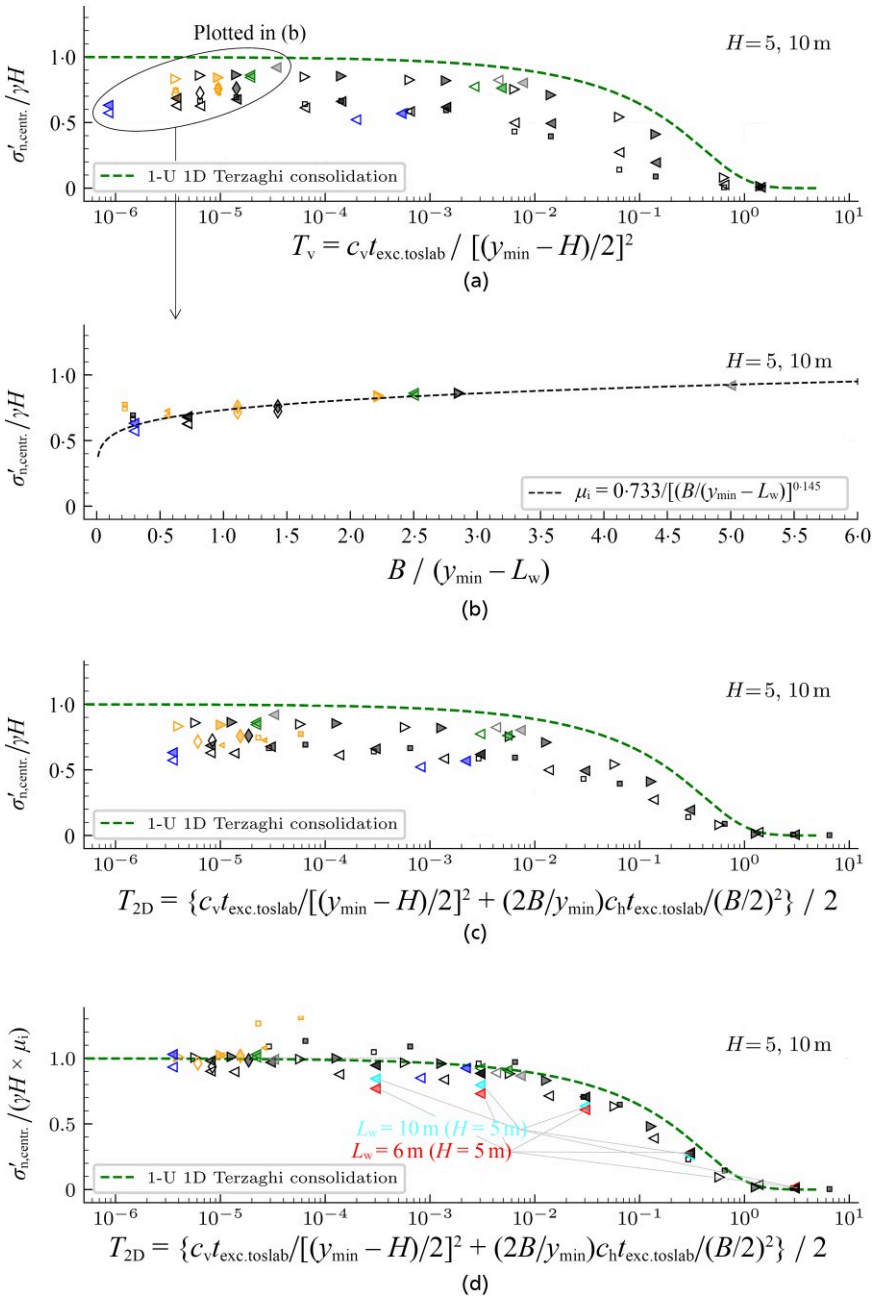

Fig. 8. Scenario 3: EHP in case of a rigid slab for H = 5 and 10 m: (a) EHP as a function of T_v; (b) EHP and influence factor μ_i; (c) EHP plotted against T_{2D}; (d) EHP normalised by μ_i and plotted against T_{2D} including influence of varying wall lengths for H = 5 m

6 (presented in the next section), it is located at 1 m depth below the ground level.

Figure 11 presents the computed EHP for five different excavation widths, with the maximum EHP occurring 5–10 years after casting of the slab. The wider the excavation, the longer the time to reach maximum EHP. The narrower the excavation, the greater is the long-term reduction of EHP due to background settlements. This scenario is, however, site specific and is only intended to demonstrate the effect of background settlements on the evolution of EHP. In summary, the maximum EHP was practically unaffected, while the long-term EHP may reduce notably due to 'down drag'.

Impact of a natural groundwater table

When developing the charts, the simulations were conducted with a groundwater table located at the excavation base, to isolate a conservative limit for the mechanism of EHP development. Compared to a more representative soft clay deposit with a groundwater table located a few metres below ground level, this introduces two oversimplifications for: (*a*) the effective stress response and hence soil stiffness and strength, and (*b*) the effect of groundwater lowering during the construction stage, as well as the subsequent regain of water pressure below the slab. Therefore, scenario 4 (without historic loading) is reanalysed with a groundwater table located at 1 m depth below ground level. Fig. 12 presents the results using the SClay1S model. In Fig. 12(a), the water pressure is set to start regaining 10 years after construction of the slab. The development of stress due to EHP is therefore allowed to proceed without being compensated by any increase in water pressure. The results of the maximum EHP in Fig. 12(a) are similar to scenario 4. The 120 years values represent the situation when the water pressures have returned and thus reduced the effective stresses.

Downloaded from http://www.emerald.com/jgeot/article-pdf/75/13/181/10972300/jgeot.24.01066en.pdf by Chalmers University of Technology user on 10 June 2026

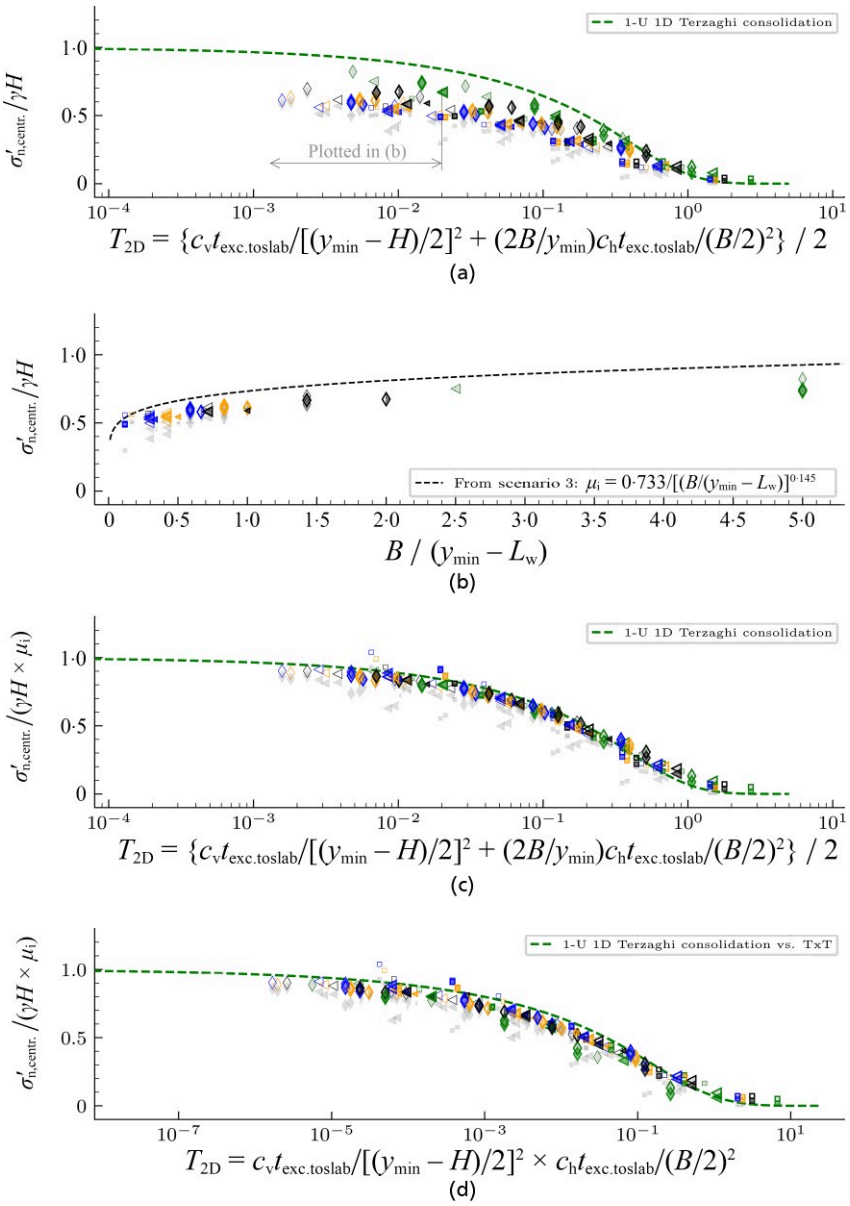

Fig. 9. Scenario 4: EHP in case of a rigid slab for H = 5 and 10 m: (a) EHP as a function of T_{2D}, (b) EHP and influence factor μ_i, (c) and (d) EHP normalised by μ_i as a function of two different T. SClay1S results are plotted using filled markers, Creep-SClay1S maximum values with unfilled markers and 120 years values are indicated by grey shaded markers

Table 5. Comparison of finite-element parametric study results to physical model test

	$EHP_{centr.}/\gamma H$	$M_{central}/\gamma HB^2$
Prototype stage 4* (Chan *et al.*, 2022a)	0·45	0·022
Prototype stage 6† (Chan *et al.*, 2022b)	0·57	0·039
Finite-element scenario 2 (BUC, MC model)	0·45–0·47 (Fig. 4)	0·020 (Fig. 7)
Finite-element scenario 3 (tunnel geometry, MC model)	0·42–0·48 (Fig. 8(d))	—
FE scenario 4 (tunnel geometry, SClay1S and CSClay1S)	0·43–0·45 (Fig. 9(c))	—

*Before applying 22 MN load on basement box.
†Long-term, 4 years after load application.

For the results shown in Fig. 12(b), the groundwater table is set to start regaining 90 days after construction of the slab. The evolution of EHP is compensated by the increase in water pressure. This is shown by the drop in maximum values compared to Fig. 12(a). The long-term stress (after 120 years) is, however, similar to that in Fig. 12(a). In addition, it should be emphasised that the design of a slab does not concern the shift of a portion of the EHP to water pressure but rather the total pressure exerted by water pressure and an additional EHP.

Comparison to field monitoring data

One simulation in Fig. 12 (see annotation) was analysed using the Creep-SClay1S model with a loading history as in scenario 5 (see scenario 6 in Fig. 10 for the computed settlement rate prior to construction). In this simulation an excavation depth H = 5 m, a span B = 20 m in a y_{min} = 90 m deep clay deposit is assumed. The time between the end of

Downloaded from http://www.emerald.com/jgeot/article-pdf/75/13/181/10972300/jgeot.24.01066en.pdf by Chalmers University of Technology user on 10 June 2026

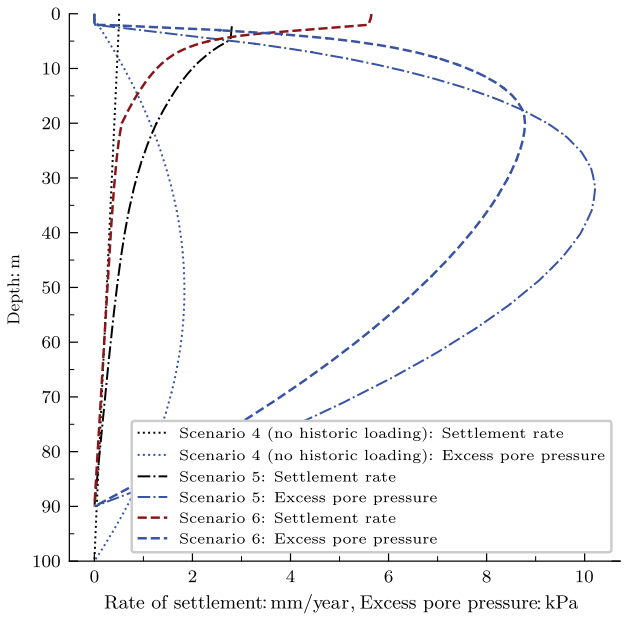

Fig. 10. Computed prior to construction settlement rates and excess pore pressures for scenarios 4, 5 and 6

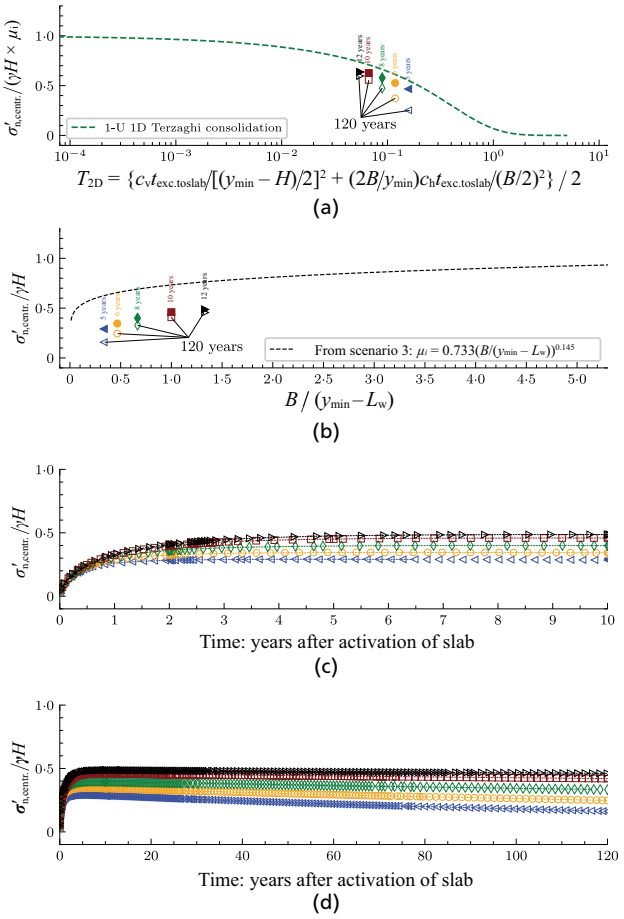

Fig. 11. Scenario 5: EHP in case of a rigid slab with significant background settlements, for H = 5 m: (a) EHP as a function of T; (b) EHP and influence factor; (c), (d) EHP plotted against time

excavation and construction of the slab $t_{exc.-slab}$ = 70 days. Pouring of the wet concrete for the slab is simulated by applying a line load for 1 day before activating the slab element. The regain of water pressure is simulated to start at

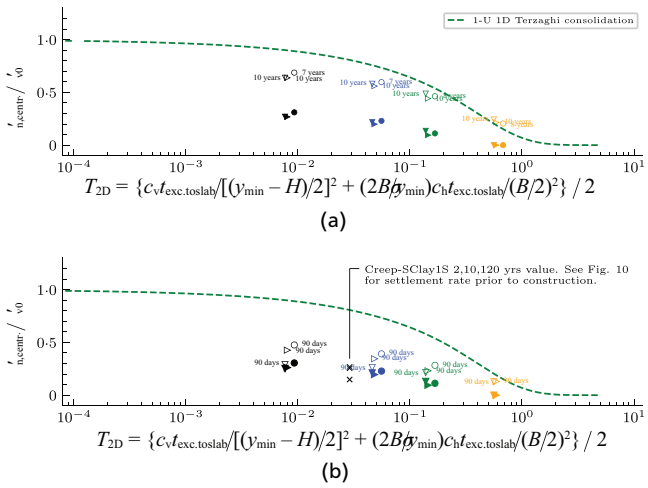

Fig. 12. Scenario 6: EHP in case of a rigid slab for H = 5 m with groundwater table located at 1 m depth b.g.l. EHP as a function of T if groundwater regains: (a) 10 years after casting of the slab; (b) after 90 days. Filled markers are 120 years after activation of slab. Unfilled markers are maximum values

180 days after casting of the slab. This resembles a specific case involving recent field monitoring of the hydro-mechanical response of soil elements below an excavation bottom in soft sensitive clay. The details of the instrumentation and the complete field monitoring data on the evolution of in situ stresses are presented in Tornborg *et al.* (2024).

The general trends of the computed response are corroborated by the monitored in situ response, as presented in Fig. 13. Some discrepancies are, however, noted. From day 0 to day 70, the measured increase in effective stress is partly due to a decrease in pore pressure. During casting of the slab, the computed increase in pore pressure is slightly less than observed. The discrepancy in computed and observed pore pressures during days 100–250 is attributed to varying dewatering activity within the pit. At day 295 there is a sudden drop in the measured vertical effective stress which offsets the measured and computed response. The general trend of the computed response is, however, satisfactory and provides partial validation of this study.

CONCLUSIONS

This paper addresses the need for a systematic study on the development of EHP at the base of deep excavations. An extensive numerical parametric study was conducted, using the finite-element method, to study the impact of normalised time T, relative stiffness R, geometry of the excavation in relation to the depth of the clay layer, retaining wall length, background settlements and location of the groundwater table, on EHP. Charts were developed using dimensionless analysis to estimate the impact of normalised time T between the end of excavation and the completion of the restraining structure at the base on the emerging magnitude of EHP for several scenarios.

Two geotechnical engineering systems of increasing complexity were studied. In addition, the complexity of the constitutive model was increased, to capture the features of natural soft clays more accurately. The scenarios studied were designed to yield a conservative value for the computed EHP; that is, the idealised supports were fully fixed once the slab was activated (i.e. zero uplift). It was shown that for flexible systems with $R < 0{\cdot}1$, the ratio EHP/σ'_{v0} may be greater than 1·0 if stiff supports/walls attract load from the mid-span. Normalised bending moments were presented as a function of

Downloaded from http://www.emerald.com/jgeot/article-pdf/75/13/181/10972300/jgeot.24.01066en.pdf by Chalmers University of Technology user on 10 June 2026

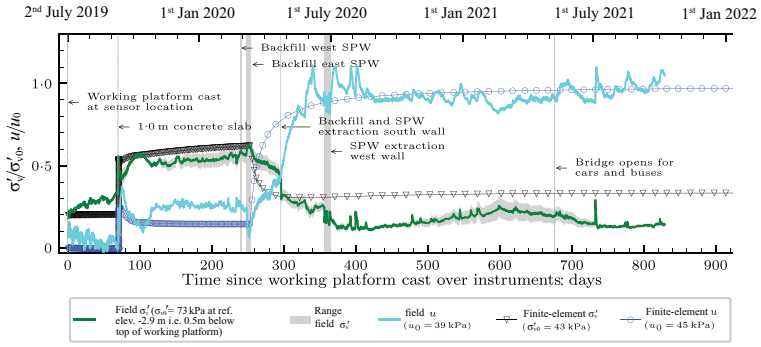

Fig. 13. Comparison of computed normalised vertical effective stress and pore pressure 0·5 m below the excavation base of a case in scenario 6 (highlighted in Fig. 12) to field monitoring data presented in Tornborg *et al.* (2024)

Table 6. Physical model test data (prototype scale).

Parameter	Value	Unit	Note
$H \times B \times L$	15 × 15 × 30	m	
y_{min}	31	m	
L_w	15	m	
w_{slab}	26	kPa	
EI_{slab}	550	MNm^2	Simulating a 'stiff' slab
σ'_{v0} at excav. base	239	kPa	
σ'_{v0} mid clay layer	298	kPa	
$E_{oed.}$ mid clay layer	20	MPa	C_s = 0·07, e_0 = 1·02
E mid clay layer	18	MPa	ν' = 0·2
$R = EI_{slab}/E_{soil}\,B^3$	0·009	—	$E_{soil} = E$
$t_{90,\ recons.centrifuge}$	40 000	hours	4 hours in model
c_v	3·8 × 10^{-7}	m^2/s	Taylor's square root of time method
$t_{excav.}$	7	weeks	
$t_{exc.–slab}$	15	weeks	
T_v	0·05 (−0·08)	—	t = 15 weeks (7 + 15 weeks)
T_{2D}	0·06 (−0·08)	—	t = 15 weeks (7 + 15 weeks)

T and R, enabling assessment of the imposed bending moment along the slab. For narrow excavations compared to the depth of the clay layer, it was shown that the EHP ratio decreases, with a minimum influence factor 0·4, purely due to geometry effects. Furthermore, as the width of the excavation reduces, it was shown that introducing a horizontal component to T_v enables the effects of 2D consolidation to be generalised. Reducing the retaining wall length imposed a maximum 20% reduction of EHP ratios.

The effects of background settlements were examined with the rate-dependent Creep-SClay1S model and it was demonstrated that, although the maximum value for EHP remains nearly unaffected, the long-term EHP reduces notably for narrow excavations due to 'down drag'. Furthermore, for a groundwater table located above the excavation base, it was shown that the returning water pressure (after dewatering) under the slab reduces the long-term EHP.

The results of the individual FE analysis and normalised charts were in good agreement with the relevant physical model tests and field monitoring data. The results of this study can, within the limitations of the scenarios studied, readily be used for estimations of EHP in preliminary design stages and as a complement to detailed project-specific analyses.

ACKNOWLEDGEMENTS

The financial support provided by Skanska, SBUF (development fund of the Swedish construction industry, grant 13995), BIG (Better Interaction in Geotechnics, grant A2021-06, from the Swedish Transport Administration) and Formas (grant 2019-00456) are gratefully acknowledged. The work was done as part of Digital Twin Cities Centre, which is supported by Sweden's Innovation Agency VINNOVA under grant no. 2019-00041. Finally, the authors would like to thank Dr Ayman Abed (Chalmers University of Technology), Dr Anders Kullingsjö and Dr Torbjörn Edstam (both at Skanska Sweden AB) for their valuable comments during the progress of this work.

APPENDIX. SUMMARY OF PHYSICAL MODEL TEST

Table 6 summarises a physical model test (Chan *et al.*, 2022a) as well as the evaluated parameter values and non-dimensional groups for the comparison presented in the section 'Comparison to physical model tests'.

NOTATION

B	excavation width
$c_{v,h}$	vertical and horizontal coefficient of consolidation, respectively
D	drainage length
E_{inc}	increase of Young's modulus with depth
E_{oed}	oedometer stiffness
E_{soil}	Young's modulus of the soil
EI_{slab}	flexural rigidity of the bottom slab

Downloaded from http://www.emerald.com/jgeot/article-pdf/75/13/181/10972300/jgeot.24.01066en.pdf by Chalmers University of Technology user on 10 June 2026

H	excavation depth
$k_{v,h}$	vertical and horizontal hydraulic conductivity (permeability), respectively
L_w	retaining wall length
M	bending moment
$M_{central}$	central bending moment of slab
M_{wall}	bending moment of slab at location of wall
OCR	overconsolidation ratio
R	non-dimensional relative stiffness ratio
T_{2D}	non-dimensional time factor considering vertical and horizontal consolidation
T_v	non-dimensional time factor for vertical consolidation
$t_{exc.-slab}$	time between the end of excavation and placement of structural element
t_{excav}	time for excavation
U	average degree of consolidation
u_0	pore pressure prior to excavation
$u_{excess,max}$	maximum excess pore pressure in the finite-element model
w	self-weight of the structural element
y_{min}	depth to bottom of clay layer
γ, γ'	unit weight, submerged unit weight
Δ_v	vertical differential displacement
δ_v	vertical displacement
μ_i	influence factor considering immediate heave
ν'	Poisson's ratio
σ'_n	effective stress normal to slab
$\sigma'_{n,centr}$	effective stress normal to slab, central part
$\sigma'_{v,h}$	vertical and horizontal effective stress, respectively
σ'_{v0}	initial vertical effective stress

REFERENCES

Bertoldo, F. & Callisto, L. (2019). Delayed response of excavations in structured clays. *Can. Geotech. J.* **56**, No. 11, 1584–1595, https://doi.org/10.1139/cgj-2018-0512.

Broere, W. (2016). Urban underground space: Solving the problems of today's cities. *Tunn. Undergr. Space Technol.* **55**, 245–248, https://doi.org/10.1016/j.tust.2015.11.012.

Brown, P. T. & Yu, S. K. R. (1986). Load sequence and structure–foundation interaction. *J. Struct. Engng* **112**, No. 3, 481–488, https://doi.org/10.1061/(ASCE)0733-9445(1986)112:3(481).

Burland, J. B. & Kalra, J. C. (1986). Queen Elizabeth II Conference Centre: geotechnical aspects. *Proc. Instn Civ. Engrs* **80**, No. 6, 1479–1503, https://doi.org/10.1680/iicep.1986.527.

Chan, D., Madabhushi, G., Nicholson, D. & Chapman, T. (2018). Twenty-one years of heave monitoring in London Clay at Horseferry Road Basement. *Ground Engng*, 9 October, https://doi.org/10.17863/CAM.33027.

Chan, D., Madabhushi, G., Viggiani, G., Williamson, M. & Hsu, Y. S. (2022a). Centrifuge modelling of the effect of base slab stiffness on long-term heave and swell pressure. *Géotechnique* **74**, No. 9, 907–919, https://doi.org/10.1680/jgeot.22.00111.

Chan, D., Madabhushi, G., Hsu, Y. S. & Tan, R. (2022b). Improving semianalytical predictions of Long-Term basement heave in over-Consolidated clay. *J. Geotech. Geoenviron. Engng* **148**, No. 2, 1–13, https://doi.org/10.1061/(asce)gt.1943-5606.0002719.

Christian, J. T. & David Carrier III, W. (1978). Janbu, Bjerrum and Kjaernsli's chart reinterpreted. *Can. Geotech. J.* **15**, No. 1, 123–128, https://doi.org/10.1139/t78-010.

Finno, R. J., Bryson, S. & Calvello, M. (2002). Performance of a stiff support system in soft clay. *J. Geotech. Geoenviron. Engng* **128**, No. 8, 660–671, https://doi.org/10.1061/(asce)1090-0241(2002)128:8(660).

Flaate, K. S. (1966). *Stresses and movements in connection with braced cuts in sand and clay*. PhD thesis, University of Illinois, Urbana, IL, USA.

Gras, J.-P., Sivasithamparam, N., Karstunen, M. & Dijkstra, J. (2018). Permissible range of model parameters for natural fine-grained materials. *Acta Geotech.* **13**, No. 2, 387–398, https://doi.org/10.1007/s11440-017-0553-1.

Ingram, P. (2012). Retaining walls as part of complete underground structure. In *ICE manual of geotechnical engineering* (eds J. Burland, T. Chapman, M. Brown and H. D. Skinner), Chapter 67, pp. 1031–1038. London, UK: ICE Publishing. https://doi.org/10.1680/moge.57098.

Karlsrud, K. & Andresen, L. (2005). Loads on braced excavations in soft clay. *Int. J. Geomech.* **5**, No. 2, 107–113, https://doi.org/10.1061/(ASCE)1532-3641(2005)5:2(107).

Karstunen, M., Krenn, H., Wheeler, S. J., Koskinen, M. & Zentar, R. (2005). Effect of anisotropy and destructuration on the behavior of Murro test embankment. *Int. J. Geomech.* **5**, No. 2, 87–97, https://doi.org/10.1061/(ASCE)1532-3641(2005)5:2(87).

Muir Wood, D. (2009). *Soil mechanics: a one-dimensional introduction*. New York, NY, USA: Cambridge University Press.

Nash, D., Lings, M. & Ng, C. (1996). Observed heave and swelling beneath a deep excavation in Gault clay. In *International symposium on geotechnical aspects of underground construction in soft ground* (eds R. J. Mair and R. Taylor). pp. 191–196. Rotterdam, the Netherlands: A.A. Balkema.

Ng, C., Hong, Y., Liu, G. & Liu, T. (2012). Ground deformations and soil–structure interaction of a multi-propped excavation in Shanghai soft clays. *Géotechnique* **62**, No. 10, 907–921, https://doi.org/10.1680/geot.10.P.072.

O'Brien, A. S., Burland, J. B. & Chapman, T. (2012). Piles and piled rafts. In *ICE manual of geotechnical engineering: Volume 2* (eds J. Burland, T. Chapman, H. Skinner and M. Brown), Chapter 56, pp. 853–885. London, UK: Thomas Telford Ltd, https://doi.org/10.1680/moge.57098.

Peck, R. B. (1943). Earth-pressure measurements in open cuts, Chicago (Il.) subway. *Trans. ASCE* **108**, No. 1, 1008–1036, https://doi.org/10.1061/TACEAT.0005647.

Peck, R. B. (1969). Deep excavations and tunnelling in soft ground. *International conference in soil mechanics and foundation engineering*, pp. 225–290.

Price, G. & Wardle, I.; BRE. (1986). Queen Elizabeth II Conference Centre: Monitoring of load sharing between piles and raft. *Proc. Instn Civ. Engrs* **80**, No. 6, 1505–1518, https://doi.org/10.1680/iicep.1986.528.,

Rouainia, M., Elia, G., Panayides, S. & Scott, P. (2017). Nonlinear finite-element prediction of the performance of a deep excavation in Boston Blue Clay. *J. Geotech. Geoenviron. Engng* **143**, No. 5, 04017005, https://doi.org/10.1061/(ASCE)GT.1943-5606.0001650.

Schweiger, H. F. & Tschuchnigg, F. (2021). A numerical study on undrained passive earth pressure. *Comput. Geotech.* **140**, 104441, https://doi.org/10.1016/j.compgeo.2021.104441.

Simpson, B. (2018). Effective heave pressures beneath restrained basement slabs. *Proc. Instn Civ. Engrs – Geotech. Engng* **171**, No. 1, 28–36, https://doi.org/10.1680/jgeen.16.00066.

Sivasithamparam, N., Karstunen, M. & Bonnier, P. (2015). Modelling creep behaviour of anisotropic soft soils. *Comput. Geotech.* **69**, No. 2015, 46–57, https://doi.org/10.1016/j.compgeo.2015.04.015.

Symons, I. F. & Tedd, P. (1989). Behaviour of a propped embedded retaining wall at Bell Common Tunnel in the longer term. *Géotechnique* **39**, No. 4, 701–710, https://doi.org/10.1680/geot.1989.39.4.701.

Tornborg, J., Karlsson, M., Kullingsjö, A. & Karstunen, M. (2021). Modelling the construction and long-term response of Göta tunnel. *Comput. Geotech.* **134**, 104027, https://doi.org/10.1139/cgj-2023-0355.

Tornborg, J., Karlsson, M. & Dijkstra, J. (2024). Temporal effective stress response of soil elements below the base of an excavation in sensitive clay. *Can. Geotech. J.* e-First, https://doi.org/10.1139/cgj-2023-0355.

United Nations (2019). World urbanization prospects: the 2018 revision. New York, NY, USA: Department of Economic and Social Affairs, Population Division, United Nations. See https://population.un.org/wup/Publications/Files/WUP2018-Report.pdf.

Whittle, A. J., Corral, G., Jen, L. C. & Rawnsley, R. P. (2015). Prediction and performance of deep excavations for courthouse station, Boston. *J. Geotech. Geoenviron. Engng* **141**, No. 4, 04014123, https://doi.org/10.1061/(asce)gt.1943-5606.0001246.

Downloaded from http://www.emerald.com/jgeot/article-pdf/75/13/181/10972300/jgeot.24.01066en.pdf by Chalmers University of Technology user on 10 June 2026